JOURNAL OF THERMOPHYSICS AND HEAT TRANSFER
Vol. 14, No. 4, October–December 2000

Measurements and Predictions of Turbulent Natural Convection Adjacent to Backward-Facing Step

B. F. Armaly,* A. Li,† H. I. Abu-Mulaweh,‡ and T. S. Chen§
University of Missouri–Rolla, Rolla, Missouri 65409

Measurements and predictions of turbulent natural convection adjacent to a two-dimensional, vertical backward-facing step in airflow are reported. The upstream and downstream walls of the backward-facing step geometry were maintained at a constant and uniform temperature, while the backward-facing step was kept adiabatic. The experiment was carried out for a backward-facing step height of 22 mm and a temperature difference, between the heated walls and the mainstream, of 30°C. Measurements and predictions of the mean velocities and temperature distributions, along with the distributions of turbulent intensities, turbulent heat fluxes, and Reynolds stress components, are presented at various axial locations downstream of the backward-facing step. A reasonable agreement appears to exist between the measured and the predicted mean quantities, but discrepancies still exist between the measured and the predicted turbulence quantities.

Nomenclature

g	=	gravitational acceleration
H	=	step height
k	=	turbulent kinetic energy
Nu_x	=	local Nusselt number based on x_ℓ, $q_w x_\ell/(\lambda \Delta T)$
P	=	modified pressure $p - \rho g x$
q_w	=	wall heat flux, $-\lambda(\partial T/\partial y)_{y=0}$
T	=	local mean temperature
T_w	=	temperature of the heated wall
T_∞	=	mainstream temperature
t	=	temperature fluctuation
$\overline{tt}$	=	intensity of temperature fluctuations
U	=	local mean streamwise velocity
u_i	=	fluctuating velocity component in the i direction
$\overline{ut}$	=	turbulent heat flux component
$\overline{uu}$	=	Reynolds normal stress component
$\overline{uv}$	=	Reynolds shear stress component
V	=	local mean transverse velocity
$\overline{vt}$	=	turbulent heat flux component
$\overline{vv}$	=	Reynolds normal stress component
x	=	streamwise distance from the step
x_ℓ	=	distance from the leading edge of the upstream wall
x_r	=	reattachment length from step
y	=	transverse distance as measured from the downstream wall
α	=	thermal diffusivity
β	=	coefficient of thermal expansion
ΔT	=	temperature difference between the heated wall and the mainstream, $(T_w - T_\infty)$
ε	=	dissipation rate of turbulent kinetic energy
θ	=	nondimensional temperature, $(T - T_\infty)/\Delta T$
λ	=	thermal conductivity
ν	=	kinematic viscosity
ν_t	=	turbulent viscosity
ρ	=	density
σ_k, σ_ε, σ_t, C_μ, $C_{\varepsilon 1}$, $C_{\varepsilon 2}$, $C_{\varepsilon 3}$, C_1	=	constants

Introduction

FLOW separation and subsequent reattachment caused by a sudden expansion in flow geometry, such as a backward-facing step, occurs in many engineering applications where heating or cooling is required. These heat transfer applications appear in electronic cooling equipment, cooling of nuclear reactors, cooling of turbine blades, combustion chambers, environmental control systems, and many other heat transfer devices. A great deal of mixing of high- and low-energy fluid occurs in the separated and reattached flow region in these devices, thus impacting their heat transfer performance. The backward-facing step geometry has been investigated extensively, both numerically and experimentally, in the laminar flow regime for natural, forced, and mixed convection flows.[1,2] On the other hand, studies of turbulent flow have dealt mainly with the forced convection case.[3–5] Some heat transfer and reattachment length measurements for turbulent natural convection flow of water has been reported by Inagaki.[6] The lack of detailed measurements or predictions of flow and thermal fields for turbulent natural convection adjacent to a backward-facing step has motivated this study. Such detailed results are needed for optimizing the performance of heat transfer devices and for developing or validating models for simulating their behaviors.

Experimental Apparatus

The air tunnel that was constructed for this experimental study is shown schematically in Fig. 1. It has a smooth converging nozzle, a straight square test section, and a smooth diverging diffuser. The tunnel was constructed from a 1.27-cm-thick Plexiglas® plate material with adequate steel frames and supports to provide a rigid structure. The transparent test section of this air tunnel allowed for optical flow visualizations and facilitated the use of a laser Doppler velocimeter (LDV) for velocity measurements. The backward-facing step geometry is supported in the test section of the tunnel and spans its entire width (85.1 cm). A cross section of 63.5 cm (28.9 step heights) by 85.1 cm (38.7 step heights) existed adjacent to the heated

Received 5 April 1999; revision received 15 January 2000; accepted for publication 4 February 2000.

*Curators' Professor, Department of Mechanical and Aerospace Engineering and Engineering Mechanics; currently Program Manager, Division of Materials Sciences and Engineering, SC 131, Office of Basic Energy Sciences, U.S. Department of Energy, 19901 Germantown Road, Germantown, MD 20874-1290.

†Graduate Research Assistant, Department of Mechanical and Aerospace Engineering and Engineering Mechanics.

‡Research Fellow, Department of Mechanical and Aerospace Engineering and Engineering Mechanics; currently Assistant Professor, Engineering Department, Purdue University at Fort Wayne, Fort Wayne, IN 46805.

§Curators' Professor, Department of Mechanical and Aerospace Engineering and Engineering Mechanics.

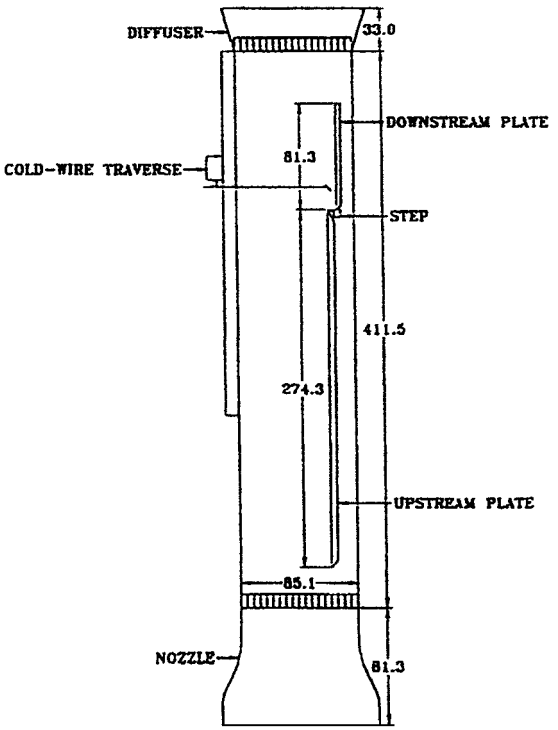

Fig. 1 Schematic of the apparatus; all dimensions are in centimeters.

walls for the developing two-dimensional boundary-layer airflow. The backward-facing step geometry is constructed with an upstream wall 274.3 cm long and a downstream wall 83.1 cm long. Both the upstream and the downstream walls can be heated to a constant and uniform temperature. The heated upstream and downstream walls are constructed from three layers that are held together by screws. The upper layer is an aluminum plate (85.1 cm wide and 1.27 cm thick) instrumented with several thermocouples that are distributed in the axial direction along its entire length. Each thermocouple is inserted into a small hole from the backside of the wall, and its measuring junction is flush with the test surface. Several thermocouples are distributed along the width of the heated wall at different axial locations for assessing uniformity of temperature in that direction. The middle layer of the heated wall consists of several heating pads that are controlled individually for the level of electrical energy input. By controlling the level of electrical energy input to each of the heating pads and monitoring the local temperature of the heated wall with the embedded thermocouples, its temperature can be maintained constant and uniform to within 0.2°C. The bottom layer of the heated wall is a 1.91-cm-thick plywood board serving as backing and support for the heated wall structure. The backward-facing step is made of Plexiglas, and it is insulated to approximate the behavior of an adiabatic surface. The front edge of the upstream wall is chamfered to ensure a proper development of the boundary-layer flow. The edges of the upstream and downstream walls, which are in contact with the step, are also chamfered to minimize the contact area with the backward-facing step and hence the conduction heat transfer between the heated walls and the step, as shown in Fig. 1.

Air velocity and temperature are measured simultaneously by using a two-component LDV and a cold-wire anemometer, respectively. The LDV system is equipped with an automated three-dimensional traverse system for positioning the measuring LDV probe volume at any desired point in the flow domain. The cold-wire probe, which is equipped with a separate traverse system, is placed within 2 mm downstream from the measuring LDV volume. With this arrangement temperature and velocity are measured simultaneously at two different points that are separated by 2 mm from each other, but are in the same plane above the heated wall. This is a weakness of this technique that could not be remedied, and its impact on the final results is negligible. The simultaneous outputs from both the LDV and the cold-wire anemometer are then processed through an A/D converter and suitable software on an IBM personal computer to determine the local instantaneous velocity and temperature. These measurements are used to determine the mean velocity and temperature, intensity of temperature fluctuations, turbulent heat flux components, Reynolds normal and shear stress components, and local Nusselt number distributions. The small separation between the velocity and temperature measuring positions (2 mm in the streamwise direction) contributes less than 2% error to the deduced local turbulent heat flux components ($\overline{ut}$ and $\overline{vt}$). The magnitude of this error depends on the streamwise gradients, which are small at most of the measured locations in this experiment.

It was established, through repeated LDV measurements, that 1024 acceptable LDV samples of the local instantaneous fluctuating velocity component are sufficient to repeatedly and accurately determine the local mean velocity in the flow domain for the experimental conditions that are described in this study. The acceptable sampling rate for these measurements varied between 10 and 100 samples per second. All of the reported data in this study represent the average values of two separate measurements taken back to back, each of which has a sample of 1024 instantaneous measurements. The repeatability of the mean velocity and temperature measurements in the separated region was determined, by using this scheme, to be within 4% and 0.25°C (0.5%), respectively. The uncertainties in the measured results are reported in the appropriate section of this paper.

The two-dimensional nature of the flow was verified through flow visualization and through measurements of velocity and temperature across the width of the air tunnel at various heights above the heated wall. These measurements displayed a wide region (65 cm or 80% of the total width of the tunnel around its center $z = 0$), where the velocity and temperature distribution, in the z direction at fixed distance from the heated wall, could be approximated (to within 5%) as uniform and two-dimensional flow. Similarly, velocity and temperature measurements were made at the center of the tunnel's width ($z = 0$) and normal to the heated wall, at various axial locations, to determine the conditions in the mainstream. These measurements reveal that the effects of the backward-facing step and the thermal conditions of the wall on the mainstream diminish at distances beyond 10 step heights (22 cm) in the transverse direction away from the heated wall. Velocity and temperature measurements in the region of 10–20 step heights (22–44 cm) in the transverse direction away from the heated wall displayed a mainstream flow region with uniform velocity and temperature distributions that are equivalent to the freestream condition of a natural convection boundary-layer flow. In addition, the flow adjacent to the unheated wall of the tunnel (wall opposite to the heated wall) was visualized to establish the existence of reversed flow in that region. These observations established that a reverse flow existed in the upper part of the tunnel in a small and very narrow region adjacent to the unheated wall. That region was very narrow, and it did not penetrate into the domain where measurements were made. All of the reported measurements were taken along the midplane ($z = 0$) of the tunnel's width and only after the system had reached steady-state conditions.

Flow visualizations were performed to verify the proper developments of the boundary layer at the starting edge of the heated wall and to observe the general nature of the flow at various axial locations. A 15-W collimated white light beam, 2.5 cm in diameter, and also a fiber optics laser light sheet were used in that process. Glycerin smoke particles, 2–5 μm in diameter, which were generated by immersing a 100-W heating element into a glycerin container, were used as scattering particles for flow visualization and also for LDV measurements.

Measurements in the air tunnel revealed that under steady-state operation the temperature of the mainstream flow increased by approximately 3°C (from 22 to 25°C) along the length of the tunnel (equivalent to 0.9°C/m). This increase in mainstream temperature along the length of the tunnel is expected because of the confining nature of the tunnel's walls. A small fraction of the energy added to the heated wall is transported to the center of the tunnel (mainstream), thus causing the temperature in that region to increase slightly with length. In the section of the tunnel where measurements were made and reported in this study (i.e., in the 25-cm region upstream from

the backward-facing step), the temperature of the mainstream increased by less than 0.25°C.

Numerical Simulation

The experimental conditions are numerically simulated by considering the domain that is shown in Fig. 2a. The heated upstream wall (2.75 m in length) and the heated downstream wall (0.8 m in length) are maintained at a uniform and equal temperature. An adiabatic backward-facing step with a height of $H = 2.2$ cm connects the upstream wall to the downstream wall. The temperature difference between the heated walls and the mainstream air flow is 30°C.

The Ince and Launder turbulence model[7] for buoyancy-driven turbulent flow is used to simulate the experimental flow and thermal conditions. The governing conservation equations can be expressed as follows:

$$\frac{\partial U_i}{\partial x_i} = 0 \tag{1}$$

$$U_j \frac{\partial U_i}{\partial x_j} = -\frac{1}{\rho}\frac{\partial P}{\partial x_i} + \frac{\partial}{\partial x_j}\left[\nu\left(\frac{\partial U_i}{\partial x_j} + \frac{\partial U_j}{\partial x_i}\right) - \overline{u_i u_j}\right] + g_i\beta(T - T_\infty) \tag{2}$$

$$U_j \frac{\partial T}{\partial x_j} = \frac{\partial}{\partial x_j}\left(\alpha\frac{\partial T}{\partial x_j} - \overline{u_j t}\right) \tag{3}$$

$$U_j \frac{\partial k}{\partial x_j} = \frac{\partial}{\partial x_j}\left[\left(\nu + \frac{\nu_t}{\sigma_k}\right)\frac{\partial k}{\partial x_j}\right] + P_k + G - \varepsilon - D \tag{4}$$

$$U_j \frac{\partial \varepsilon}{\partial x_j} = \frac{\partial}{\partial x_j}\left[\left(\nu + \frac{\nu_t}{\sigma_\varepsilon}\right)\frac{\partial \varepsilon}{\partial x_j}\right] + \frac{\varepsilon}{k}(C_{\varepsilon 1}P_k + C_{\varepsilon 3}G - C_{\varepsilon 2}f_\varepsilon\varepsilon) + E + Y \tag{5}$$

where

$$-\overline{u_i u_j} = \nu_t\left(\frac{\partial U_i}{\partial x_j} + \frac{\partial U_j}{\partial x_i}\right) - \frac{2}{3}k\delta_{ij}$$

$$-\overline{u_j t} = \frac{1.5C_\mu f_\mu}{\sigma_t}\frac{k}{\varepsilon}\overline{u_j u_k}\frac{\partial T}{\partial x_k} \tag{6}$$

$$P_k = -\overline{u_i u_j}\frac{\partial U_i}{\partial x_j}, \qquad G = -g_i\beta\overline{u_i t}$$

$$\nu_t = C_\mu f_\mu \frac{k^2}{\varepsilon}, \qquad D = 2\nu\left(\frac{\partial k^{\frac{1}{2}}}{\partial x_j}\right)^2 \tag{7}$$

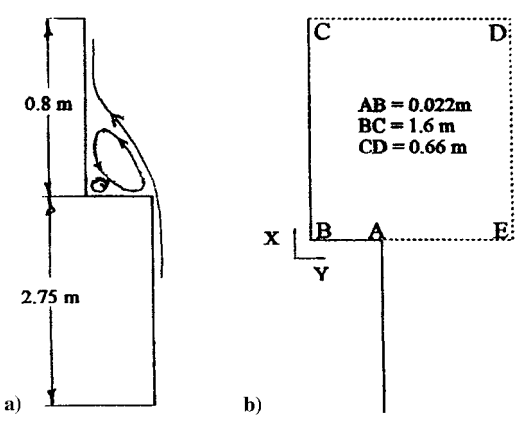

Fig. 2 Schematic of physical and computational domain.

$$E = 2\nu\nu_t\left(\frac{\partial^2 U_i}{\partial x_j \partial x_k}\right)^2, \qquad \varepsilon = \nu\left(\frac{\partial u_i}{\partial x_j}\right)^2 - 2\nu\left(\frac{\partial k^{\frac{1}{2}}}{\partial x_j}\right)^2$$

$$Y = 0.83\left(\frac{k^{\frac{3}{2}}}{\varepsilon C_l y} - 1\right)\left(\frac{k^{\frac{3}{2}}}{\varepsilon C_l y}\right)^2\frac{\varepsilon^2}{k} \tag{8}$$

$$f_\mu = \exp\left[-\frac{3.4}{(1 + R_t/50)^2}\right], \qquad f_\varepsilon = \left[1 - 0.3\exp\left(-R_t^2\right)\right]$$

$$R_t = \left(\frac{k^2}{\nu\varepsilon}\right) \tag{9}$$

The computational domain used in the simulation is shown in Fig. 2b. The inlet section (A–E) is placed at the step, and the exit section (C–D) is placed at 1.6 m downstream from the step. To minimize the effects of the imposed outlet boundary conditions on the flow near the step, the length of the downstream heated wall is increased in the simulation to 1.6 m (twice the experimental value). The width of the outlet section (C–D) was taken as 0.635 m, equivalent to the experimental conditions. The boundary conditions for this geometry are as follows:

1) At the solid walls (A–B–C), $U = V = k = \varepsilon = 0$, $T = T_w$ on B–C, and $(\partial T/\partial x)_{x=0} = 0$ on A–B.

2) At the inlet section (A-E), measured values were used, where k was considered to be equal to $\overline{uu}$ and ε was determined from the computed profiles of natural convection along a vertical flat plate at that section.

3) At the outlet section (C–D), $\partial U/\partial x = \partial V/\partial x = \partial T/\partial x = \partial k/\partial x = \partial\varepsilon/\partial x = 0$.

4) At the mainstream (E–D), $U = 0$, $\partial V/\partial y = 0$, $T = T_\infty$, and small values were assigned for k and ε (10^{-25}).

5) The coefficients appearing in the model are as follows: $\sigma_t = 0.9$, $\sigma_k = 1.0$, $\sigma_\varepsilon = 1.3$, $C_{\varepsilon 1} = 1.44$, $C_{\varepsilon 2} = 1.92$, $C_{\varepsilon 3} = 1.44$, $C_\mu = 0.09$, and $C_1 = 2.5$.

The preceding turbulence model was implemented in a finite volume computational fluid dynamics code utilizing the SIMPLER algorithm. A nonuniform grid system is used in the computational domain. The grid is highly concentrated in the recirculating flow region. Two different grid systems, with $NX \times NY = 255 \times 148$ and 128×75, were tested for the experimental geometry, and the results for the reattachment length (x_r), along with the maximum values of the Nusselt number (Nu_x), velocity, and turbulent kinetic energy, were compared at three streamwise locations $x/H = 0.5$, 1.0, and 3.0. None of these results deviated by more than 5%. As a result, the finer grid system was used in the present simulation. Thermophysical properties of air were treated as constants and evaluated at the average film temperature of 35°C, and the Boussinesq approximation was used to evaluate the buoyancy term.

Results and Discussion

The operation of the air tunnel, its instrumentation, along with the accuracy and the repeatability of the measurements were validated by performing measurements of turbulent natural convection boundary-layer flow adjacent to an isothermal vertical heated flat plate. The upstream heated wall of the present backward-facing step geometry served as the test surface for these measurements. Both measured flow and thermal fields for this case compared very favorably with those reported by Cheesewright and Mirzai[8] as shown in Abu-Mulaweh et al.[9] This validates the performance of the air tunnel and its instrumentation.

The general flow behavior, as predicted, downstream of the step is illustrated in Fig. 3 for the region that is close to the step. The upstream flow detaches at the sharp upper corner of the step, forming a free shear layer. The region that is far away from the step (10–20 step heights in the transverse direction) is not shown in Fig. 3, and the flow in that region is not affected by the step. That region is designated as the mainstream region. The separating shear layer curves sharply toward the downstream wall. Part of the separating shear-layer fluid is deflected upstream into a recirculating flow region by

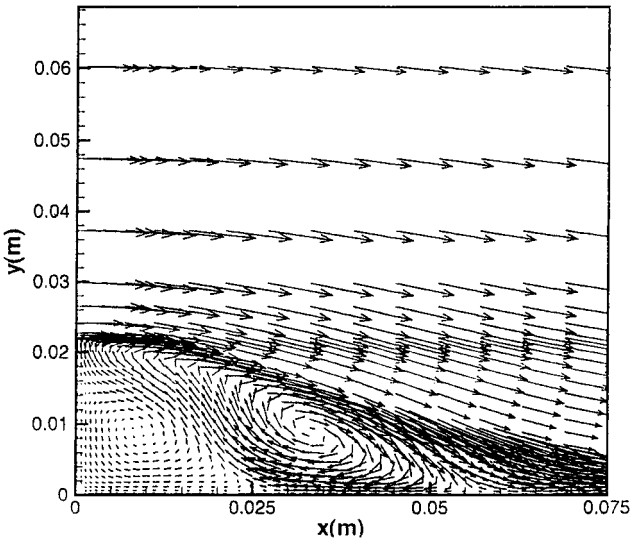

Fig. 3 Predicted flow patterns.

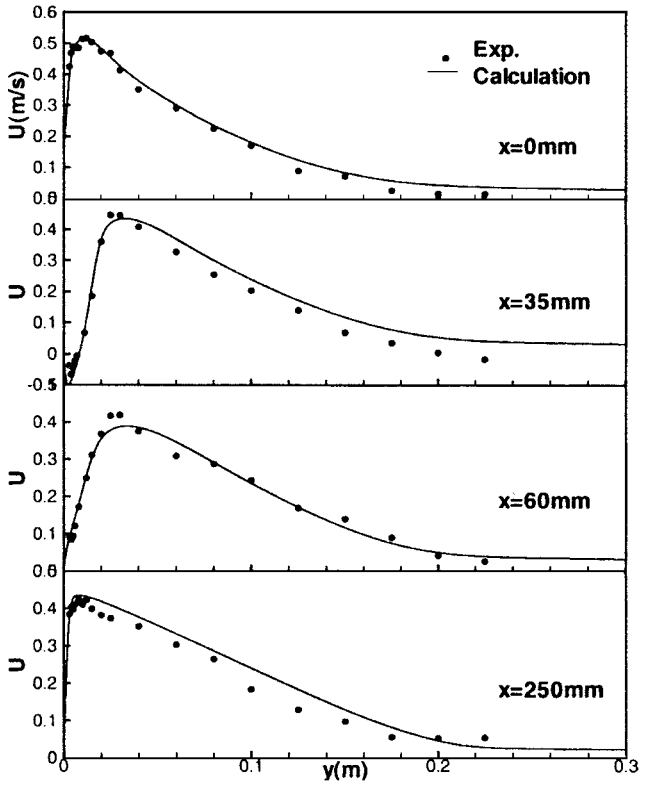

Fig. 4 Local mean streamwise velocity. (Uncertainty in y is 0.1 mm and in U is 3%.)

a strong adverse pressure gradient. Downstream of reattachment a new sub-boundary layer begins to grow up through the reattached layer. Part of the reversed flow is deflected again toward the bottom corner of the step to form a secondary recirculating flow region. The two recirculating flow regions are clearly observed in Fig. 3. The secondary flow region is larger in size than its equivalent for forced convection flow primarily because of the buoyancy-assisting force. The predicted reattachment length for the experimental conditions is $x_r = 6.8$ cm ($x_r / H = 3.1$). Experimental observations reveal that the reattachment length is not steady, and it oscillates in the region between $5.5 < x_r < 6.5$ cm and that compares well with predictions. Measurements that are reported in this region represent the average value resulting from these oscillations.

A comparison between the predicted and measured local mean streamwise velocity distributions is presented in Fig. 4. The profile

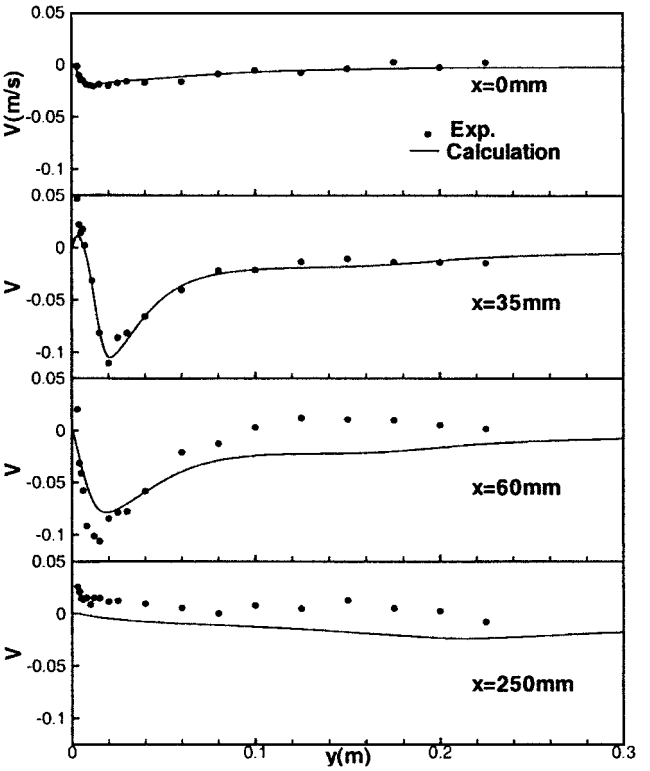

Fig. 5 Local mean transverse velocity. (Uncertainty in y is 0.1 mm and in V is 3%.)

at $x = 0$ corresponds to the inlet boundary condition in the numerical simulation. For the results at $x = 0$, the normal distance y is measured from the surface of the upstream wall. The predicted results downstream from the step are seen to compare favorably with measured values. The velocity distribution at $x = 3.5$ cm exhibits negative values close to the heated wall because that plane is in the recirculating flow region. The maximum local mean streamwise velocity decreases as the distance from the step increases up to the reattachment region because of the sudden expansion in geometry, and then starts to increase as the distance from the step continues to increase because of the buoyancy-assisting force. The distance between the wall and the maximum velocity position becomes smaller, and the wall shear stress becomes larger as the distance from the step continues to increase. The uncertainties in the measurements are 0.1 mm in y, 1 mm in x, and 3% in U.

A comparison between the predicted and measured local mean transverse velocity distributions is presented in Fig. 5. Here again the profile at $x = 0$ corresponds to the inlet boundary condition in the numerical simulation. The predicted results compare favorably with measured data, with the maximum deviation occurring in the outer region of the reattached flow ($x = 25$ cm), where the magnitude of that velocity component is very small and the sensitivity to measurements error is large. All of the local mean transverse velocity distributions exhibit negative values at the outer edge of the recirculating flow region, indicating flow entrainment from the main fluid stream into that region. In addition, the local mean transverse velocities in the very narrow region close to the heated wall are always positive. The effect of the step has diminished at $x = 25$ cm, and the flow downstream of that location can be approximated as developing boundary-layer flow. The local mean streamwise velocity distribution at that cross section, in Fig. 4, confirms that behavior. The figure also shows that in the recirculating flow region ($x = 3.5$ cm) the local mean transverse velocity component is positive when the local mean streamwise velocity component is negative. The uncertainty in the measured values for V is 3%.

A comparison between the predicted and measured nondimensional local mean temperature distributions θ is presented in Fig. 6. The predicted results compare favorably with measured values. A kink in the temperature distribution can be observed at $x = 3.5$ and

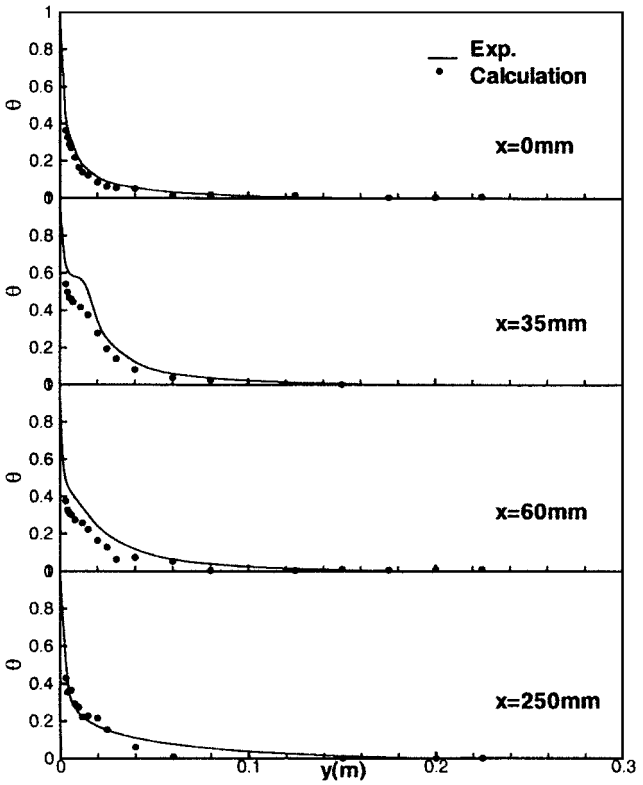

Fig. 6 Local mean dimensionless temperature. (Uncertainty in y is 0.1 mm and in θ is 1%.)

6.0 cm, which is caused by the shear layer that bounds the recirculating flow region. The temperature distribution asymptotically approaches the mainstream temperature as the distance from the heated wall increases. The local heat flux for the heated downstream wall was determined from the measured local temperature distribution (temperature gradient at the wall) inside the laminar sublayer that is adjacent to the heated wall. The air temperature was measured at four different locations within 0.5 mm from the wall, by the cold-wire anemometer, in order to determine the local temperature gradient at the heated wall. The data from these temperature measurements could not be displayed in Fig. 6 because of scale limitations. Air temperature distributions in the laminar sublayer near the heated wall were linear, and the temperature fluctuation in that region was very small (near zero). The local air temperature gradient at the wall was used to determine the local heat flux q_w and the local Nusselt number Nu_x. This method for determining the wall temperature gradient and the Nusselt number in turbulent flow was used successfully also by Qiu et al.[10] The local Nusselt number distribution deduced from these measured temperature gradients compares favorably with the predicted values, as shown in Fig. 7. In the region close to the step, the magnitude of the local Nusselt number is lower than that of a flat plate (reaching a minimum), and that is because of the relatively low flow velocities that occur in the secondary recirculating flow region. The Nusselt number increases with increasing distance from the step, reaching a maximum value of almost twice that of a flat plate in the vicinity of the reattachment region. The impact of the relatively cooler fluid from the shear layer on the heated wall and the deflection of cooler fluid into the primary recirculating flow region cause this rapid increase in the Nusselt number. The magnitude of the local Nusselt number decreases and asymptotically approaches the flat-plate value as the distance continues to increase in the streamwise direction. The uncertainty in the measured values for the temperature T is 0.05°C, for the wall temperature T_w is 0.2°C, for θ is 1%, and for the Nusselt number Nu_x is 6%.

Comparisons between the measured and predicted results for the Reynolds normal stress components $\overline{uu}$ and $\overline{vv}$ and for the intensity of the temperature fluctuations $\overline{tt}$ are presented in Figs. 8, 9, and 10, respectively. The turbulence model that is used in the simulation

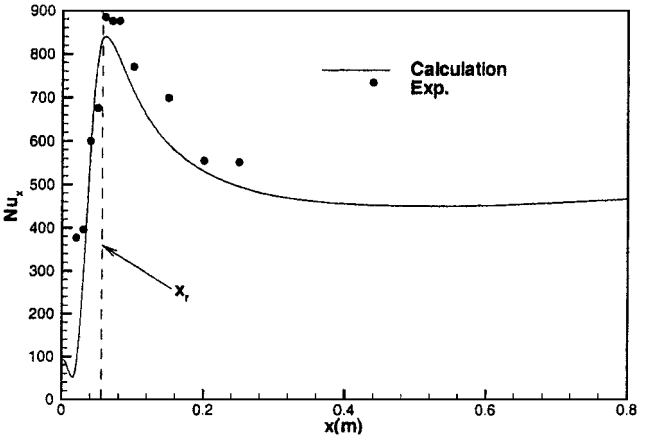

Fig. 7 Local Nusselt number. (Uncertainty in x is 1 mm and in Nu_x is 6%.)

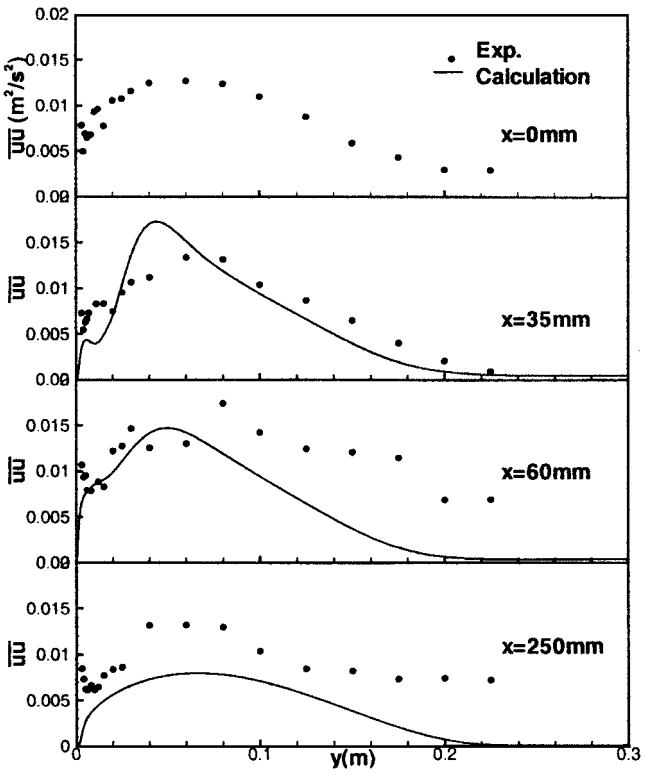

Fig. 8 Reynolds normal stress component $\overline{uu}$. (Uncertainty in y is 0.1 mm and in $\overline{uu}$ is 6%.)

does not predict the intensity of the temperature fluctuations, and for that reason Fig. 10 contains only measured values. Predicted and measure values in Figs. 8 and 9 appear to have similar trends, but the difference between them is significant. These results show that the Reynolds normal stress components and the intensity of temperature fluctuations, at any streamwise location, increase to a maximum as the transverse distance from the heated surface increases. They start to decrease as the transverse distance from the heated surface continues to increase, reaching a minimum value in the mainstream. The maximum of the two Reynolds normal stress components, at any streamwise location, appears to occur at approximately the same distance from the heated wall, but the location of the maximum intensity of the temperature fluctuations appears to occur at a closer distance. The uncertainty in the measured results are 6% in $\overline{uu}$, 6% in $\overline{vv}$, and 4% in $\overline{tt}$.

A comparison between the measured and predicted Reynolds shear stress component $\overline{uv}$, turbulent heat flux components $\overline{ut}$, $\overline{vt}$ are presented in Figs. 11, 12, and 13, respectively. Predicted values

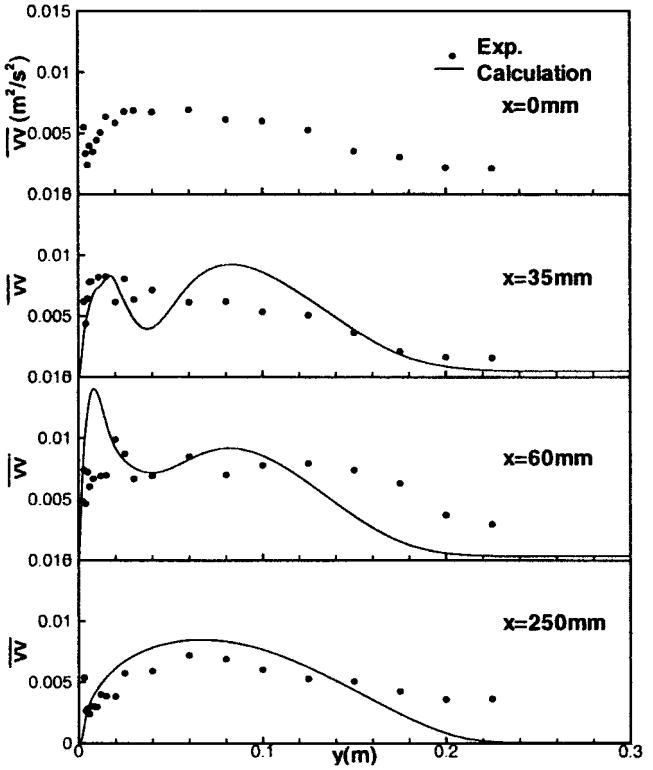

Fig. 9 Reynolds normal stress component $\overline{vv}$. (Uncertainty in y is 0.1 mm and in $\overline{vv}$ is 6%.)

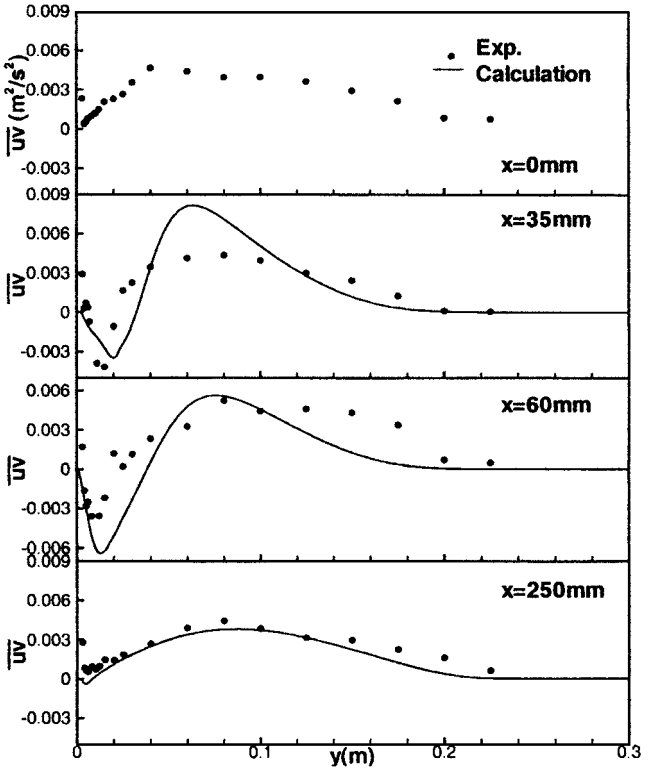

Fig. 11 Reynolds shear stress component $\overline{uv}$. (Uncertainty in y is 0.1 mm and in $\overline{uv}$ is 6%.)

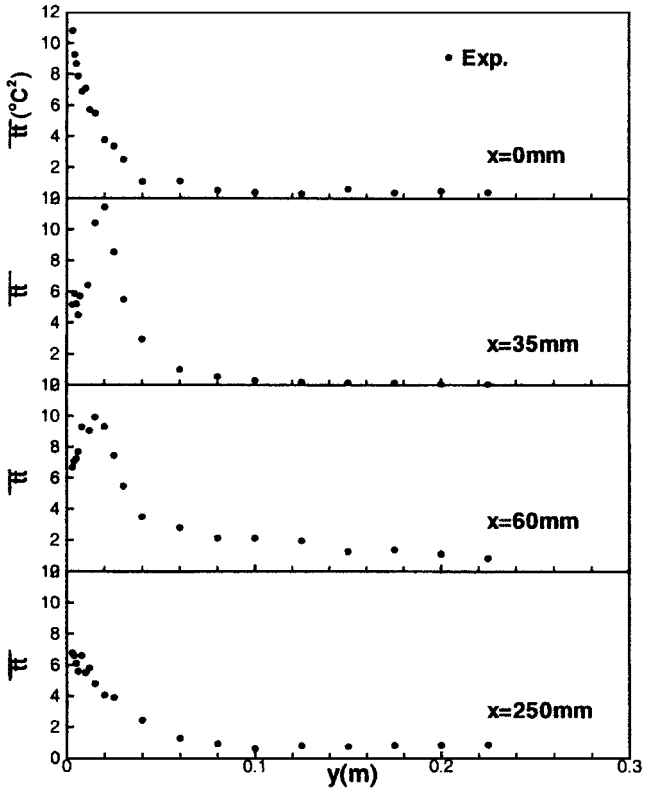

Fig. 10 Intensity of temperature fluctuations. (Uncertainty in y is 0.1 mm and in $\overline{tt}$ is 4%.)

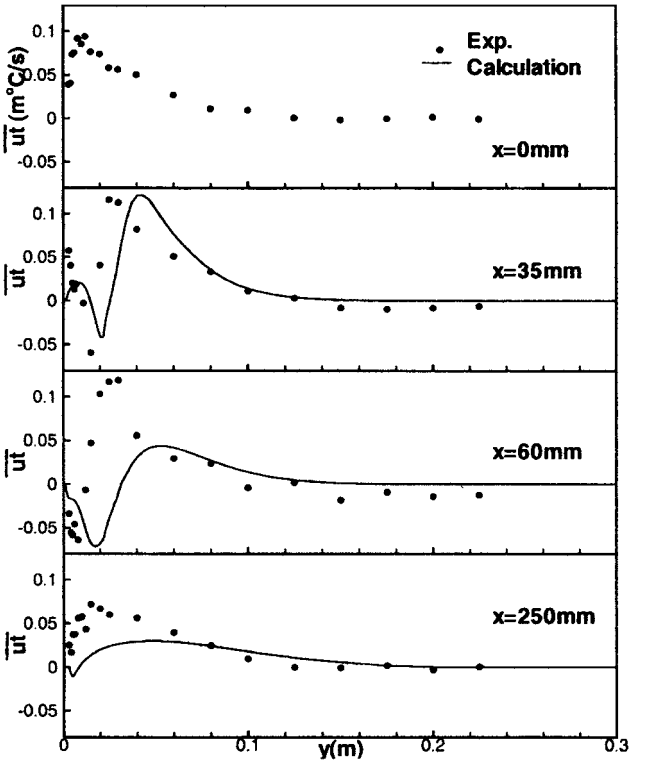

Fig. 12 Turbulent heat flux component $\overline{ut}$. (Uncertainty in y is 0.1 mm and in $\overline{ut}$ is 6%.)

Table 1 Turbulent natural convection over a backward-facing step and temperature and velocity measurements ($x = 0$ cm, $H = 22$ mm, $\Delta T = 30°C$)

y, mm	U, m/s	V, m/s	T, °C	$\overline{uu}$, m^2/s^2	$\overline{vv}$, m^2/s^2	$\overline{uv}$, m^2/s^2	$\overline{tt}$, °C^2	$\overline{ut}$, m/s°C	$\overline{vt}$, m/s°C
3	0.4243	−0.0016	40.9000	0.0078	0.0055	0.0023	10.7800	0.0392	0.0270
4	0.4679	−0.0101	39.7500	0.0049	0.0033	0.0004	9.2500	0.0404	0.0419
5	0.4874	−0.0148	38.6800	0.0069	0.0024	0.0006	8.6560	0.0735	0.0380
6	0.4841	−0.0151	38.0600	0.0065	0.0040	0.0008	7.8650	0.0755	0.0596
8	0.4844	−0.0188	36.5100	0.0068	0.0035	0.0010	6.8880	0.0918	0.0613
10	0.5133	−0.0196	34.9200	0.0093	0.0044	0.0012	7.0910	0.0854	0.0701
12	0.5151	−0.0205	34.1300	0.0096	0.0051	0.0015	5.7080	0.0939	0.0532
15	0.5030	−0.0186	33.6600	0.0077	0.0064	0.0021	5.4860	0.0766	0.0772
20	0.4738	−0.0201	32.5200	0.0106	0.0059	0.0023	3.7660	0.0741	0.0560
25	0.4677	−0.0175	31.8400	0.0108	0.0068	0.0027	3.3500	0.0580	0.0539
30	0.4131	−0.0158	31.6200	0.0116	0.0069	0.0036	2.5040	0.0561	0.0503
40	0.3515	−0.0172	31.5300	0.0125	0.0068	0.0047	1.0750	0.0501	0.0376
60	0.2910	−0.0161	30.3600	0.0127	0.0070	0.0044	1.1230	0.0271	0.0181
80	0.2264	−0.0088	30.5700	0.0124	0.0062	0.0040	0.5299	0.0112	0.0120
100	0.1718	−0.0053	29.9900	0.0110	0.0060	0.0040	0.3956	0.0094	0.0073
125	0.0892	−0.0074	30.4500	0.0088	0.0053	0.0037	0.2942	0.0005	0.0012
150	0.0729	−0.0037	29.9000	0.0059	0.0035	0.0030	0.5905	−0.0018	−0.0006
175	0.0266	0.0027	30.1600	0.0043	0.0031	0.0022	0.3604	−0.0003	0.0004
200	0.0162	−0.0024	30.1500	0.0030	0.0022	0.0009	0.4830	0.0016	−0.0030
225	0.0160	0.0025	30.2700	0.0029	0.0021	0.0008	0.3859	−0.0006	−0.0047

Table 2 Turbulent natural convection over a backward-facing step and temperature and velocity measurements ($x = 3.5$ cm, $H = 22$ mm, $\Delta T = 30°C$)

y, mm	U, m/s	V, m/s	T, °C	$\overline{uu}$, m^2/s^2	$\overline{vv}$, m^2/s^2	$\overline{uv}$, m^2/s^2	$\overline{tt}$, °C^2	$\overline{ut}$, m/s°C	$\overline{vt}$, m/s°C
3	−0.0375	0.0464	47.1900	0.0073	0.0062	0.0029	5.1560	0.0573	0.0112
4	−0.0668	0.0218	45.9200	0.0055	0.0044	0.0003	5.8610	0.0405	0.0408
5	−0.0450	0.0144	44.9600	0.0063	0.0064	0.0007	5.1970	0.0201	0.0362
6	−0.0223	0.0174	44.7400	0.0066	0.0078	0.0004	4.4810	0.0130	0.0463
7	−0.0061	0.0021	44.3100	0.0073	0.0079	−0.0007	5.6990	0.0189	0.0401
11	0.0672	−0.0316	43.4600	0.0083	0.0082	−0.0039	6.4070	−0.0030	0.0568
15	0.1849	−0.0816	42.2300	0.0083	0.0082	−0.0042	10.4100	−0.0594	0.1171
20	0.3598	−0.1104	39.3000	0.0075	0.0062	−0.0011	11.4300	0.0408	0.0887
25	0.4467	−0.0860	36.7900	0.0095	0.0081	0.0017	8.5430	0.1161	0.0936
30	0.4454	−0.0815	35.2000	0.0107	0.0064	0.0023	5.4930	0.1127	0.0760
40	0.4081	−0.0658	33.4500	0.0112	0.0071	0.0034	2.9450	0.0819	0.0547
60	0.3277	−0.0405	32.1500	0.0134	0.0061	0.0041	0.9881	0.0508	0.0283
80	0.2548	−0.0221	31.7700	0.0132	0.0062	0.0044	0.5443	0.0333	0.0156
100	0.2038	−0.0214	30.9400	0.0104	0.0054	0.0039	0.2879	0.0111	0.0068
125	0.1395	−0.0135	30.9100	0.0087	0.0051	0.0030	0.1918	0.0031	0.0044
150	0.0683	−0.0106	31.0200	0.0065	0.0036	0.0024	0.1423	−0.0083	−0.0034
175	0.0356	−0.0136	30.9200	0.0040	0.0021	0.0013	0.1217	−0.0097	−0.0017
200	0.0042	−0.0140	30.8200	0.0021	0.0016	0.0001	0.0546	−0.0083	−0.0027
225	−0.0171	−0.0146	30.7900	0.0009	0.0016	0.0001	0.0340	−0.0062	−0.0029

Table 3 Turbulent natural convection over a backward-facing step and temperature and velocity measurements ($x = 6$ cm, $H = 22$ mm, $\Delta T = 30°C$)

y, mm	U, m/s	V, m/s	T, °C	$\overline{uu}$, m^2/s^2	$\overline{vv}$, m^2/s^2	$\overline{uv}$, m^2/s^2	$\overline{tt}$, °C^2	$\overline{ut}$, m/s°C	$\overline{vt}$, m/s°C
3	0.0914	0.0203	41.24	0.0107	0.0074	0.0017	6.664	−0.034	0.016
4	0.0835	−0.0318	39.7900	0.0094	0.0046	−0.0016	7.0690	−0.0558	0.0300
5	0.0934	−0.0413	39.2400	0.0095	0.0072	−0.0028	7.2150	−0.0588	0.0171
6	0.1203	−0.0578	39.0100	0.0079	0.0060	−0.0025	7.6800	−0.0461	0.0113
8	0.1716	−0.0916	38.1900	0.0079	0.0067	−0.0036	9.2770	−0.0642	0.0256
12	0.2491	−0.1012	37.6900	0.0088	0.0069	−0.0036	9.0460	−0.0069	0.0455
15	0.3110	−0.1061	36.6600	0.0083	0.0069	−0.0022	9.9190	−0.0470	0.0549
20	0.3674	−0.0843	34.9000	0.0122	0.0099	0.0012	9.3000	0.1031	0.0446
25	0.4168	−0.0787	33.8200	0.0128	0.0087	0.0002	7.4270	0.1172	0.0583
30	0.4184	−0.0777	31.8700	0.0147	0.0067	0.0012	5.4610	0.1188	0.0630
40	0.3754	−0.0582	32.2000	0.0126	0.0069	0.0023	3.4850	0.0555	0.0367
60	0.3089	−0.0211	31.5900	0.0130	0.0085	0.0033	2.7860	0.0293	0.0300
80	0.2871	−0.0126	30.1200	0.0174	0.0070	0.0052	2.1290	0.0238	0.0152
100	0.2431	0.0031	29.9100	0.0142	0.0078	0.0044	2.1240	−0.0040	0.0116
125	0.1690	0.0120	30.1200	0.0125	0.0079	0.0046	1.9540	0.0018	−0.0121
150	0.1397	0.0108	30.3200	0.0121	0.0074	0.0043	1.2480	−0.0185	−0.0171
175	0.0902	0.0099	30.2100	0.0115	0.0063	0.0034	1.3660	−0.0090	−0.0140
200	0.0415	0.0053	30.3100	0.0069	0.0037	0.0007	1.1030	−0.0140	−0.0149
225	0.0261	0.0019	30.3200	0.0069	0.0029	0.0005	0.8366	−0.0125	−0.0036

Table 4 Turbulent natural convection over a backward-facing step and temperature and velocity measurements ($x = 25$ cm, $H = 22$ mm, $\Delta T = 30°C$)

y, mm	U, m/s	V, m/s	T, °C	$\overline{uu}$, m^2/s^2	$\overline{vv}$, m^2/s^2	$\overline{uv}$, m^2/s^2	$\overline{tt}$, °C^2	$\overline{ut}$, m/s°C	$\overline{vt}$, m/s°C
3	0.3848	0.0259	43.88	0.0085	0.0054	0.0028	6.766	0.0251	0.0185
4	0.4036	0.0210	41.6200	0.0073	0.0026	0.0008	6.5920	0.0167	0.0230
5	0.3969	0.0146	41.8700	0.0062	0.0028	0.0006	6.1030	0.0373	0.0306
6	0.4099	0.0136	41.9100	0.0061	0.0024	0.0005	5.5770	0.0374	0.0315
8	0.4236	0.0152	39.7600	0.0066	0.0030	0.0009	6.5910	0.0560	0.0405
10	0.4100	0.0087	39.1700	0.0061	0.0030	0.0007	5.4920	0.0576	0.0332
12	0.4233	0.0151	37.6100	0.0065	0.0040	0.0009	5.7930	0.0430	0.0470
15	0.3987	0.0149	37.7800	0.0077	0.0038	0.0014	4.7750	0.0717	0.0403
20	0.3820	0.0116	37.4400	0.0084	0.0038	0.0014	4.0540	0.0667	0.0342
25	0.3733	0.0123	35.6100	0.0086	0.0057	0.0019	3.8960	0.0599	0.0455
40	0.3520	0.0097	32.8300	0.0131	0.0059	0.0027	2.4250	0.0562	0.0407
60	0.3034	0.0055	31.2800	0.0132	0.0072	0.0039	1.2720	0.0397	0.0310
80	0.2650	0.0003	30.9800	0.0130	0.0069	0.0044	0.9139	0.0246	0.0147
100	0.1834	0.0079	30.8500	0.0104	0.0060	0.0039	0.5997	0.0095	0.0063
125	0.1288	0.0047	30.9800	0.0084	0.0053	0.0031	0.7855	−0.0000	−0.0026
150	0.0973	0.0128	31.0100	0.0082	0.0051	0.0030	0.7340	−0.0008	−0.0044
175	0.0555	0.0050	30.9800	0.0073	0.0042	0.0022	0.8114	0.0019	−0.0050
200	0.0523	0.0025	31.0000	0.0074	0.0036	0.0016	0.8189	−0.0030	−0.0060
225	0.0531	−0.0079	31.0300	0.0072	0.0036	0.0006	0.8346	0.0006	−0.0061

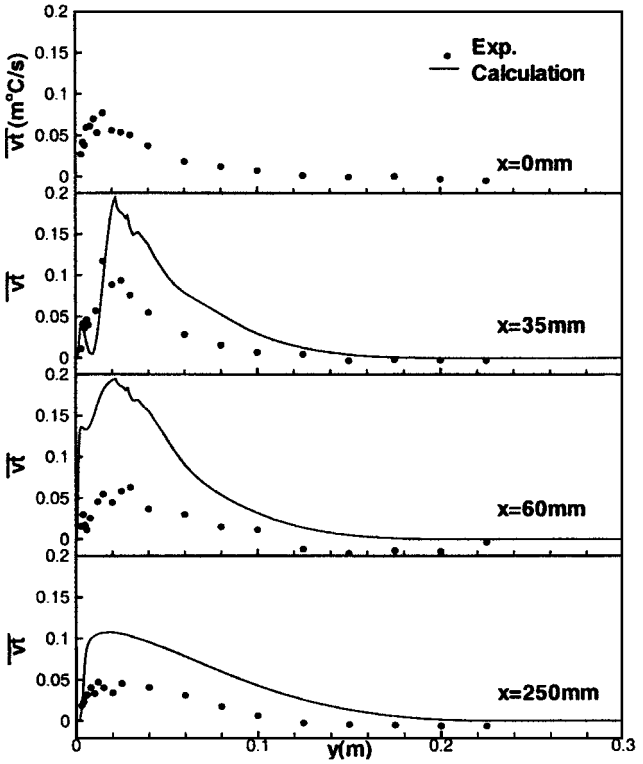

Fig. 13 Turbulent heat flux component $\overline{vt}$. (Uncertainty in y is 0.1 mm and in $\overline{vt}$ is 6%.)

appear to have similar trend as the measured values, but the difference in their magnitudes is significant. A minimum and a maximum appear to exist in their distributions in the plane where recirculating flows exist ($x = 3.5$ cm), and they all are of the same order of magnitude. The magnitude decreases, after its maximum value, asymptotically to zero in the mainstream. The maximum in the transverse component of the turbulent heat flux distribution $\overline{vt}$ occurs at approximately the same distance from the wall as the maximum for the intensity of the temperature fluctuations. The uncertainty in these measured values for $\overline{uv}$, $\overline{ut}$, and $\overline{vt}$ is 6%.

All of the graphically reported results are also presented in tabular form (Tables 1–5) for use in future comparison with other numerically simulated results for this geometry and experimental conditions.

Table 5 Turbulent natural convection over a backward-facing step and Nusselt number measurements ($H = 22$ mm, $\Delta T = 30°C$)

X, cm	Nu_x
2	377
3	396
4	600
5	676
6	885
7	876
8	876
10	770
15	699
20	555
25	552

Conclusions

Measurements and predictions of the flow and thermal fields in turbulent natural convection adjacent to a vertical two-dimensional backward-facing step are presented. The general behavior of the results is similar to that of separated forced convection flow adjacent to such a geometry. The maximum local Nusselt number, which is approximately twice that of the flat-plate value at similar flow conditions, occurs in the reattachment region. For the experimental conditions the reattachment region is not steady, and its center varies between 5.5 and 6.5 cm or 2.5–2.95 step heights. Predictions compare favorably with measurements of mean quantities (velocity, temperature, Nusselt number, and reattachment length), but the turbulent fluctuating quantities do not fair that well. Other turbulence models should be explored for the purpose of providing a better comparison with the fluctuating quantities.

Acknowledgments

This work was supported in part by the National Science Foundation under Grants CTS-9304485, CTS-9906746, and CTS-9818203.

References

[1] Abu-Mulaweh, H. I., Armaly, B. F., and Chen, T. S., "Laminar Natural Convection Flow over a Vertical Backward-Facing Step," *Journal of Heat Transfer*, Vol. 117, No. 4, 1995, pp. 895–901.

[2] Abu-Mulaweh, H. I., Armaly, B. F., and Chen, T. S., "Measurements in Buoyancy-Assisting Laminar Boundary Layer Flow over a Vertical Backward-Facing Step—Uniform Wall Heat Flux Case," *Experimental*

Thermal and Fluid Science, Vol. 7, No. 1, 1993, pp. 39–48.

[3]Abe, K., Kondoh, T., and Nagano, Y., "A New Turbulence Model for Predicting Fluid Flow and Heat Transfer in Separating and Reattaching Flows—I: Flow Field Calculations," *International Journal of Heat and Mass Transfer*, Vol. 37, No. 1, 1994, pp. 139–151.

[4]Abe, K., Kondoh, T., and Nagano, Y., "A New Turbulence Model for Predicting Fluid Flow and Heat Transfer in Separating and Reattaching Flows—II: Thermal Field Calculations," *International Journal of Heat and Mass Transfer*, Vol. 38, No. 8, 1995, pp. 1467–1481.

[5]Vogel, J. C., and Eaton, J. K., "Combined Heat Transfer and Fluid Dynamic Measurements Downstream of a Backward-Facing Step," *Journal of Heat Transfer*, Vol. 107, No. 4, 1985, pp. 922–929.

[6]Inagaki, T., "Heat Transfer and Fluid Flow of Turbulent Natural Convection Along a Vertical Flat Plate with a Backward-Facing Step," *Experimental Heat Transfer*, Vol. 7, No. 4, 1994, pp. 285–301.

[7]Ince, N. Z., and Launder, B. E., "On the Computation of Buoyancy Driven Turbulent Flows in Rectangular Enclosures," *International Journal of Heat and Fluid Flow*, Vol. 10, No. 2, 1989, pp. 110–117.

[8]Cheesewright, R., and Mirzai, M. H., "The Correlation of Experimental Velocity and Temperature Data for a Turbulent Natural Convection Boundary Layer," *Proceedings of the 2nd U.K. National Conference on Heat Transfer*, Inst. of Mechanical Engineers, London, 1988, pp. 79–89.

[9]Abu-Mulaweh, H. I., Armaly, B. F., and Chen, T. S., "Measurement of Turbulent Natural Convection Flow over a Vertical Backward-Facing Step," *The Proceedings of 1996 International Mechanical Engineering Congress and Exposition*, HTD-333(2), American Society of Mechanical Engineers, New York, Inst. of Mechanical Eng., London, 1996, pp. 313–321.

[10]Qiu, S., Simon, T. W., and Volino, R. J., "Evaluation of Local Wall Temperature, Heat Flux, and Convective Heat Transfer Coefficient from the Near-Wall Temperature Profile," *Proceedings of 1995 National Heat Transfer Conference*, HTD-318, American Society of Mechanical Engineers, New York, 1995, pp. 45–52.